

# Spatio-temporal behavior of Spiral Vortex Flow

M. Heise, D. Küter, J. Abshagen, and G. Pfister

Institute of Experimental and Applied Physics, University of Kiel, 24098 Kiel, Germany

E-mail: heise@physik.uni-kiel.de

**Abstract.** Experimental realizations of Taylor-Couette flow often include rigid end plates at bottom and top of the system. As a consequence of such end plates the bifurcation behavior of the basic laminar flow as well as the spatio-temporal properties of the emerging pattern, such as e.g. spiral vortex flow, can change. The latter point is in the focus of our present experimental study. The spatio-temporal behavior of spiral vortex flow in a Taylor-Couette system with rigid end plates is analyzed by a measurement technique based on Doppler-shift. This enables us to determine the spatial amplitude profile of up- and downward propagating spiral vortices within oscillatory flow states. Our study confirms experimentally recent numerical results of Hoffmann *et al.* [1] on the spatio-temporal properties of the spiral vortex state in finite systems with rigid end plates.

## 1. Introduction

The Taylor-Couette system is one of the classical systems for the study of bifurcation events and nonlinear pattern formation [2–7]. It is the flow of a viscous fluid in the gap between two concentric and independently rotating cylinders. Circular Couette flow (CCF) is the basic laminar flow under the mathematical assumption of infinite axial length (or axial periodic boundary conditions) of the system. It has a translational invariance and reflection symmetry in axial as well as rotational invariance in azimuthal direction, i.e. the flow is invariant under the group  $O(2) \times SO(2)$  [7,8]. For sufficiently high rates of counter-rotation non-axisymmetric 'pure' spiral vortices occur in CCF via a symmetry-breaking Hopf bifurcation with  $O(2)$  symmetry as a result of linear instability [9,10]. These spirals are traveling waves in axial and rotating waves in azimuthal direction and have an azimuthal wave number  $m = \pm 1$  for the parameter values considered here. Spiral vortices have been first theoretically calculated by Krueger *et al.* [11] and experimentally observed by Snyder [12]. Experimental as well as combined numerical and experimental studies on counter-rotating Taylor-Couette flow have been carried out by Andereck *et al.* [13] and Langford *et al.* [10], respectively. In these studies spiral vortices have been observed as first time-dependent pattern that appears from basic laminar flow for a wide range of counter-rotation rates in systems with different radius ratios and axial length. Numerical studies on spirals focusing on their nonlinear behavior have been performed by Sanchez *et al.* [14] and Hoffmann *et al.* [15].

Non-rotating rigid end plates at top and bottom as often used in experimental systems break the translational invariance. It has been predicted theoretically [16,17] that a Hopf bifurcation with broken translational invariance differ from its counterpart for infinite systems. Due to broken translational invariance, standing waves (SW) appear supercritically instead of spiral vortices. Spiral vortices arise exclusively super- or subcritically from a secondary

steady bifurcation of the SW solutions. Experimental investigations on Taylor-Couette flow reveal such a difference in the bifurcation behavior for sufficiently small aspect-ratios [18]. As a further consequence non-rotating rigid end plates at top and bottom subcritically innervate axisymmetric Ekman vortices in the annulus. Recent numerical simulations have shown that 'pure' spiral vortices only exist in a bulk region which is bound by a 'wavy-like' rotating defects in the vicinity of the axisymmetric Ekman vortices near the end plates [1]. Spiral vortices in finite systems are therefore predicted to differ qualitatively in their spatio-temporal properties from 'pure' spirals in infinite systems. An experimental investigation of the spatio-temporal behavior of this flow state is the focus of the present work.

## 2. Experimental setup

The Reynolds number of the inner and the outer cylinder serve as control parameters  $Re_{i,o} = (r_o - r_i)r_{i,o}\Omega_{i,o}/\nu$ , where  $\Omega_{i,o}$  and  $r_{i,o}$  denotes the angular velocity and radius of the inner ( $i$ ) and the outer ( $o$ ) cylinder, respectively. The inner cylinder of the apparatus is machined from stainless steel having a radius of  $r_i = (12.50 \pm 0.01)$  mm, while the outer cylinder is made from optically polished glass with a radius of  $r_o = (25.00 \pm 0.01)$  mm. The gap width  $d$  between the inner and outer cylinder is  $d = r_o - r_i = 12.5$  mm. The working fluid is a silicone oil with a kinematic viscosity  $\nu = 10.6$  cSt which is thermostatically controlled to  $(24.00 \pm 0.01)^\circ\text{C}$ . The flow is confined in axial direction by two rigid end plates having a distance  $L$  which defines the axial length of the system. The dimensionless geometric parameters are the aspect ratio  $\Gamma = L/d$  and the radius ratio  $\eta = r_i/r_o$ . In this study the radius ratio is held fixed at  $\eta = 0.5$  and all of the measurements have been performed at  $\Gamma = 12$  using flow visualization and Laser Doppler velocimetry (LDV) for measurements of the local flow velocity. All LDV measurements are recorded at a radial distance of 1 mm from the inner cylinder.

## 3. Results

In this work a measurement technique based on Doppler-shift is used in order to study the spatio-temporal behavior of oscillatory flow states. This kind of measurements have been performed by recording the axial velocity  $v_z(t)$  of the flow by LDV while simultaneously moving the LDV in axial direction from top to bottom. Thereby the axial position  $z(t) = v_{LDV}t$  of the LDV is given by the axial scan velocity  $v_{LDV}$  and each data point represents a certain time  $t$  referring to a distinct axial position  $z(t)$ . Three of these so-called 'axial scans' recorded from different flow states are depicted in figure 1. Each of these measurements represents a typical flow state that appears in counter-rotating Taylor-Couette flow with rigid end plates.  $Re_o$  is held constant at  $-120.0$  during all measurements presented here.

The axial scan in figure 1(a) has been recorded at  $Re_i = 114.5$  and is referred to basic flow. The fact that the lines of this scan are thin (compared to the ones in (b) and (c)) denotes that the flow is stationary. The Ekman vortices at bottom (left side) and top (right side) decay into the bulk as typically observed for  $Re_o = 0$  [19, 20]. In the axial middle of the system the axial velocity  $v_z$  is zero. By increasing  $Re_i$  above a critical value this stationary flow state becomes unstable and a new flow state appears. An axial scan referring to this time dependent flow state is depicted in figure 1(b). Especially at top and bottom the stationary Ekman vortex profile is still visible as thin lines, but in addition to that an oscillation of the axial velocity can be seen in the bulk of the system. Note, that this oscillation appears as broad black band in this representation due to the small scan velocity ( $v_{LDV} = 0.1$  mm/s).

Within the oscillatory regime in the bulk also nodal points are visible in this axial scan. In these nodal points, the axial velocity  $v_z$  is constant which is a strong indicator for SW [21]. In (c) an axial scan referring to downward traveling spiral vortices is depicted. The Ekman vortices at bottom and top are still visible and appear as thin line in this scan. In contrast to the axial scan in (b) the nodal points have disappeared in the bulk and due to the oscillation as well

as the above mentioned small scan velocity a broad black band appears. This band includes (almost) constant amplitude especially in the vicinity of axial mid height.

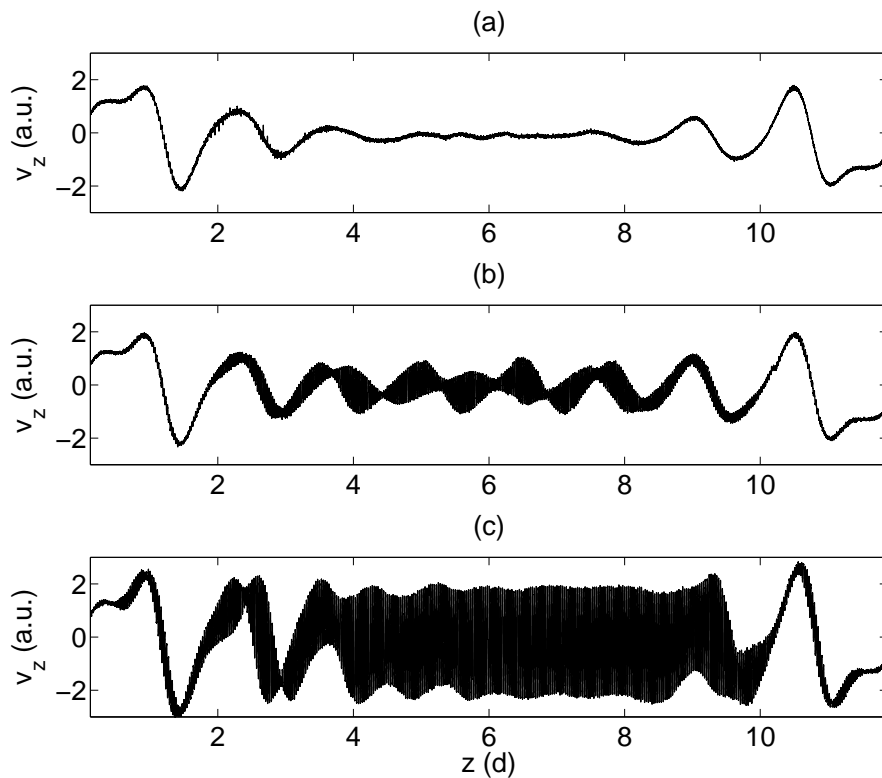


**Figure 1.** Axial scans of three different flow states recorded at  $Re_o = -120.0$ : (a) basic flow at  $Re_i = 114.5$ , (b) standing waves (SW) at  $Re_i = 115.3$  and (c) downward traveling spiral (R-SPI) at  $Re_i = 120.4$ .

This sequence of states is typically observed in the parameter regime considered here as a part of a bifurcation scenario [22]. Apart from basic flow each time-dependent flow state, e.g., SW and spirals, will be studied in the following by separating dominant frequencies from each other in the power spectrum which appear due to the Doppler-shift based measurement technique. This separation procedure will be presented in detail in the following and is a suitable method for analyzing the spatio-temporal behavior of the oscillatory flow.

The axial scan of SW (shown also in figure1(b)) is again depicted in figure 2(a). Additionally to that, the power spectrum of this scan is displayed in (c). Beside one peak at lower frequencies ( $f_{Ek} \approx 0.02$  Hz) which belongs to the Ekman vortex structure two other frequency peaks are visible in the spectrum. These peaks correspond to the up- and downward traveling spiral modes respectively. Both peaks are identical for the case that the LDV measurement volume is held fixed at a constant axial position, but due to the axial motion of the LDV apparatus from top to bottom each frequency is Doppler-shifted toward either a higher or a lower frequency. The frequency of the upward traveling L-SPI-mode (blue dashed line) is shifted toward higher whereas the downward traveling R-SPI-mode (red dashed line) is shifted toward lower frequencies. The difference between these two frequencies is directly related to the axial velocity of the LDV measurement system. Note, that the Ekman vortices are stationary (no oscillation) and the

corresponding frequency peak in (c) simply reflects the axial motion of the LDV measurement volume. The result of a (narrow) bandpass-filtering of the two spiral mode frequencies can be seen in figure 2(b). For reasons of clarity both signals are artificially separated by an offset from zero, e.g.,  $-1.0$  for L-SPI-mode (blue) and  $+1.0$  for R-SPI-mode (red). Additionally propagation directions of both spiral modes are indicated by two white arrows in this plot. The amplitude of each spiral mode, estimated by the bandpass-filtered axial scan, is similarly distributed over the whole bulk of the system. Here the amplitudes of both spiral modes are not exactly equal as it would be expected for SW. However, slightly asymmetric SW can appear within the transition sequence from SW to spiral vortices [16, 17, 23]. This behavior is also in agreement with recent results of numerical simulation of the Navier-Stokes equation by Hoffmann *et al.* [1].

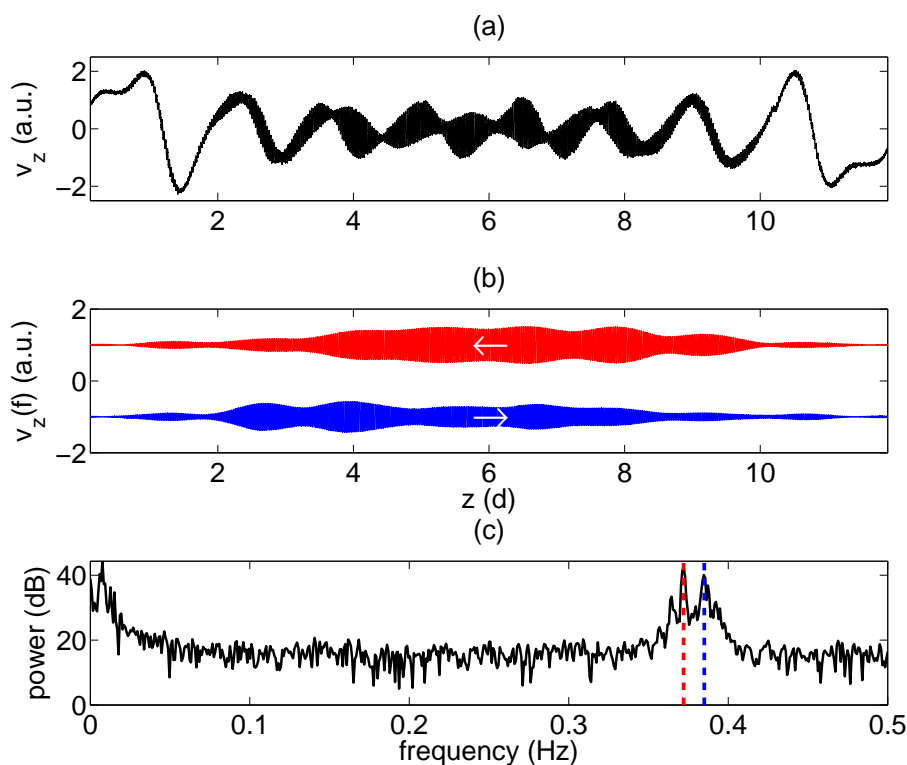


**Figure 2.** (a) Axial scan of a standing wave (SW) recorded at  $Re_o = -120.0$  and  $Re_i = 115.3$ , (b) spatially resolved bandpass-filtered scan of (a) red: R-SPI-mode ( $0.360 - 0.378$  Hz, offset:  $+1.0$ ) and blue: L-SPI-mode ( $0.378 - 0.400$  Hz, offset:  $-1.0$ ) and (c) power spectrum of (a) - the lines mark the corresponding frequencies in (b).

Analogue to the analysis of SW, also the axial scan of a downward traveling spirals R-SPI (as already shown in figure 1(c)) is analyzed in the following. The axial scan of this flow state is depicted in figure 3(a) and the power spectrum of this scan is shown in (c). In addition to the frequency peak of the Ekman vortex structure ( $f_{Ek} \approx 0.02$  Hz) also the double peak for up- (L-SPI-mode: blue dashed line) and downward traveling spiral modes (R-SPI-mode: red dashed line) exist. As discussed above this double peak is observed due to the Doppler-shift which results of the axial motion of the LDV system during this measurement, e.g., frequency peak of the downward (upward) traveling spiral mode is shifted to lower (higher) frequencies.

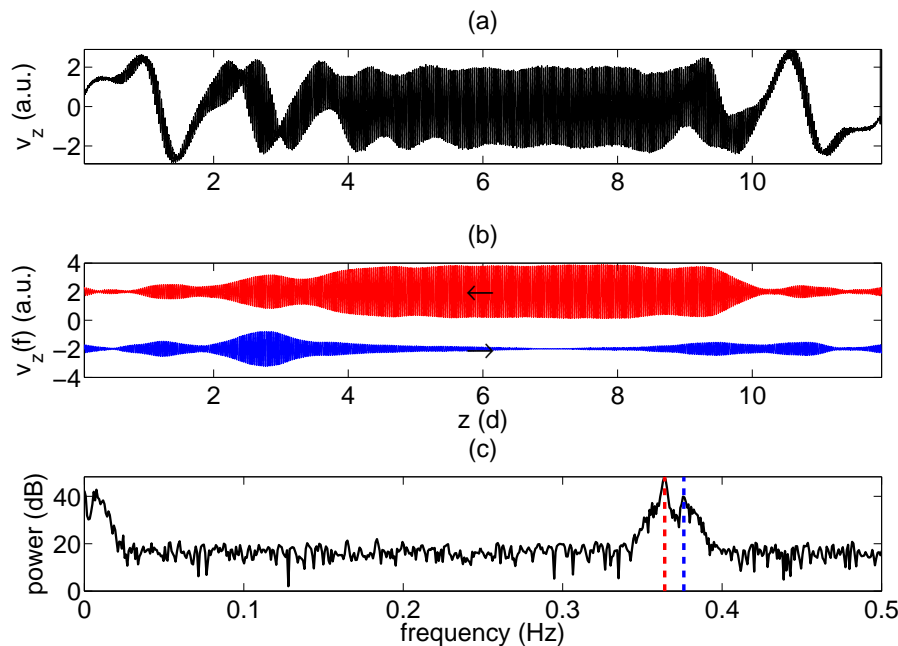


**Figure 3.** (a) Axial scan of a downward traveling spiral (R-SPI) recorded at  $Re_o = -120.0$  and  $Re_i = 120.0$ , (b) spatially resolved bandpass-filtered scan of (a) red: R-SPI-mode (0.350 – 0.371 Hz, offset:+2.0) and blue: L-SPI-mode (0.371 – 0.390 Hz, offset:-2.0) and (c) power spectrum of (a) - the lines mark the corresponding frequencies in (b).

This implies that not only the downward traveling R-SPI-mode but also the upward traveling L-SPI-mode exists in this flow state. This is also verified in the bandpass-filtered scans for both spiral modes, that are depicted in (b). For reasons of clarity both bandpass-filtered axial scans are artificially separated by an offset, e.g., R-SPI-mode (red – offset:+2.0) and L-SPI-mode: (blue – offset:-2.0). The black arrows additionally indicate the axial propagation direction of each spiral mode. As expected, the amplitude of R-SPI-mode is dominant in the bulk, whereas the amplitude of L-SPI-mode is nearly zero in this region. But the amplitudes of both types of spiral modes are almost equal in the vicinity of the end plates and decay directly at the end plates. Especially at the bottom end plate, where the phase of R-SPI-mode is annihilated, the amplitudes of both modes are almost equal and form together with the Ekman vortex structure a 'wavy-like' flow in this regime as numerically observed by Hoffmann *et al.* [1]. This structure can even be observed in (a) and a nodal point, as typically observed for SW, exist at  $z \approx 3d$ . This dynamical behavior differs systematically from that of 'pure' spirals in Taylor-Couette flow with axial periodic boundary conditions (or infinite length) but is in qualitative agreement with recent numerical simulation of the Navier-Stokes equation considering rigid end plates [1].

Not only the downward traveling R-SPI but also the upward traveling L-SPI exist in counter-rotating Taylor-Couette flow and can appear from SW by (spontaneous) breaking of the reflection symmetry. In figure 4(a) and (c) axial scans of both coexisting spirals are depicted, e.g., the upward traveling L-SPI (a) and the downward traveling R-SPI (c). The propagation direction is schematically indicated by the arrows in each plot. In addition to that also parts of the corresponding power spectra are depicted in (b) for L-SPI and in (d) for R-SPI. In both spectra the typical double peaks of the spiral modes are visible. In each case (L-SPI (a) or R-SPI (c)) either the higher peak corresponding to L-SPI-mode or the lower one of R-SPI-mode has more

spectral power density, e.g., in (b) the peak of L-SPI-mode and in (d) the R-SPI-mode peak is larger. Note, that by applying a point reflection in the axial middle of the system ( $z = 6d$ ) both axial scans can be converted into each other.

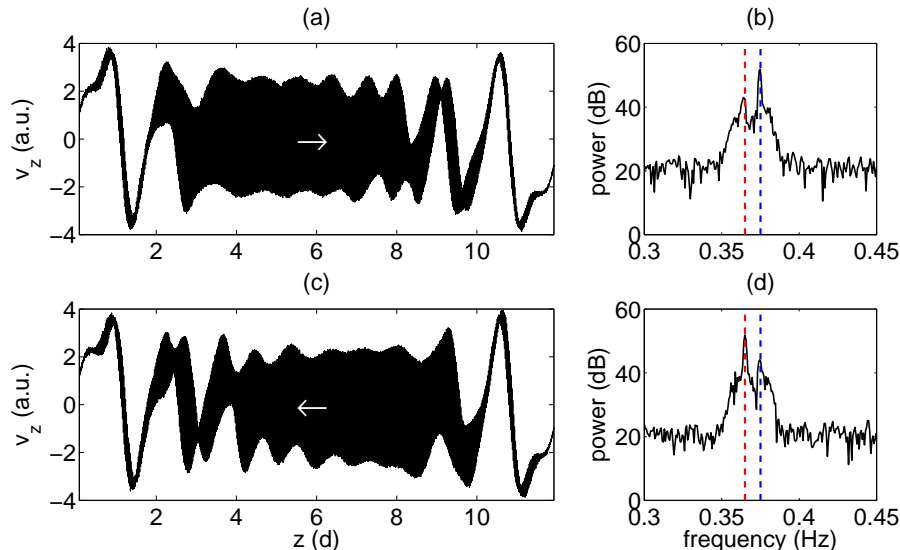


**Figure 4.** Axial scans of oppositely traveling spirals measured at  $Re_o = -125.0$  and  $Re_i = -120.0$ : (a) upward traveling spiral L-SPI and (c) downward traveling spiral R-SPI and power spectra of (a) and (c) are depicted in (b) for L-SPI (a) and (d) for R-SPI (c). The red (blue) dashed line indicates the peak of R-SPI-mode (L-SPI-mode).

#### 4. Conclusions

In this experimental study we have analyzed the spatio-temporal behavior of different oscillatory states that occur in the bifurcation sequences from basic flow via standing waves to spiral vortex flow in counter-rotating Taylor-Couette flow with rigid end plates. The behavior of each flow state is analyzed experimentally by using a measurement technique that is based on Doppler-shifted signals of axial scans. This technique allows us to decompose the oscillatory flow into axially traveling waves, here up- and downward traveling spirals, and yield a spatial amplitude distribution of each type of traveling wave. We found that spirals in experimental Taylor-Couette systems with rigid end plates consist of both types of 'pure' spiral modes, i.e. up- and downward traveling spirals, having similar amplitudes near each end plate but with one type dominating in the bulk of the system. The results are in qualitative agreement with theoretical considerations [16,17] and recent numerical Navier-Stokes simulations [1].

#### Acknowledgments

We acknowledge support from the Deutsche Forschungsgemeinschaft.

#### 5. References

- [1] Hoffmann C, Lücke M and Pinter A 2005 *Phys. Rev. E* **72** 056311
- [2] DiPrima R C and Swinney H L 1981 *Instabilities and transition in flow between concentric cylinders* (Springer-Verlag) p 139
- [3] Guckenheimer J and Holmes P 1986 *Nonlinear Oscillations, Dynamical Systems and Bifurcations of Vector Fields* (Springer-Verlag)
- [4] Cross M C and Hohenberg P C 1993 *Rev. Mod. Phys.* **65** 851
- [5] Tagg R 1994 *Nonlinear Science Today* **4** 1–25

- [6] Egbers C and Pfister G 2000 *Physics of rotating fluids* (Springer Verlag, Berlin)
- [7] Chossat P and Iooss G 1994 *The Couette-Taylor Problem* (Springer-Verlag)
- [8] Golubitsky M and Stewart I 1986 *SIAM Journal of Mathematical Analysis* **17** 249
- [9] Golubitsky M and Langford W F 1988 *Physica D* **32** 362–392
- [10] Langford W F, Tagg R, Koestlich E J, Swinney H L and Golubitzky M 1988 *Phys. Fluids* **31** 776–785
- [11] Krueger E R, Gross A and di Prima R C 1966 *J. Fluid Mech.* **24** 521
- [12] Snyder H A 1968 *Phys. Fluids* **11** 728–734
- [13] Andereck C D, Lui S S and Swinney H L 1986 *J. Fluid Mech.* **164** 155–183
- [14] Sanchez J, Crespo D and Marques F 1993 *Appl. Sci. Res.* **51** 55–59
- [15] Hoffmann C and Lücke M 2000 *Physics of rotating fluids* ed Egbers C and Pfister G (Springer Verlag, Berlin) pp 55–66
- [16] Landsberg A S and Knobloch E 1996 *Phys. Rev. E* **53** 3579–3600
- [17] Dangelmayr G and Knobloch E 1991 *Nonlinearity* **4** 399–427
- [18] Langenberg J, Pfister G and Abshagen J 2003 *Phys. Rev. E* **68** 056308
- [19] Pfister G and Rehberg I 1981 *Phys. Lett. A* **83** 19
- [20] Roth D, Lücke M, Kamps M and Schmitz R 1992 *Ordered and Turbulent Patterns in Taylor-Couette Flow* vol B297 ed Andereck D and Hayot F (NATO ASI Series, Plenum, New York) pp 59–66
- [21] Abshagen J, Langenberg J, Pfister G, Mullin T, Tavener S J and Cliffe K A 2004 *Theo. Comp. Fluid Dyn.* **18** 129 – 136
- [22] Langenberg J, Pfister G and Abshagen J 2004 *Phys. Fluids* **16** 2757–2762
- [23] Langenberg J, Pfister G and Abshagen J 2004 *Phys. Rev. E* **70** 046209